Homodyne measurement of the average photon number

J. G. Webb,[1] T. C. Ralph,[2] and E. H. Huntington[1]
[1]*Centre for Quantum Computer Technology, School of Information Technology and Electrical Engineering, University College, The University of New South Wales, Canberra, Australian Capital Territory 2600, Australia*
[2]*Centre for Quantum Computer Technology, Department of Physics, The University of Queensland, St Lucia, Queensland 4072, Australia*
(Received 17 January 2006; published 13 March 2006)

We describe a scheme for measurement of the mean photon flux at an arbitrary optical sideband frequency using homodyne detection. Experimental implementation of the technique requires an acousto-optic modulator in addition to the homodyne detector, and does not require phase locking. The technique exhibits polarization and frequency and spatial mode selectivity, as well as much improved speed, resolution, and dynamic range when compared to linear photodetectors and avalanche photodiodes, with potential application to quantum-state tomography and information encoding using an optical frequency basis. Experimental data also support a quantum-mechanical description of vacuum noise.

DOI: 10.1103/PhysRevA.73.033808 PACS number(s): 42.50.Xa, 42.50.Ar

I. INTRODUCTION

A fundamental optical measurement is the intensity of a specific mode. The application of the theory of quantum mechanics to optical fields tells us that for a given optical mode the intensity is quantized [1], appearing as a discrete photon flux. For a sufficiently small flux the individual photons can be resolved and counted using a number of standard techniques such as avalanche photodiodes (APDs), photomultipliers, and bolometers [2]. The optimum approach for a given application is dependent upon the wavelength and expected photon flux. An important point is that at optical frequencies the thermal background is at zero temperature to an excellent approximation [3]. Thus "dark counts," i.e., photon events in the absence of illumination, are technical in nature.

It is also possible to probe an optical mode by first mixing it with a strong reference field, a local oscillator, before detecting its intensity. This is called homodyne detection. In this case detection is generally by linear positive-intrinsic-negative (*p-i-n*) photodiode detectors which cannot resolve individual photons. Instead, the continuous spectrum of the signal's quadrature amplitudes is measured. These quadrature amplitudes exhibit zero-temperature fluctuations [1], and a noise floor is thus observed for homodyne detection in the absence of signal illumination.

Although all this is well known and the performance of photon counters and homodyne detectors has been tested individually for many systems [4], to our knowledge a direct comparison of the photon counting and homodyne signal of the same field has not been made. In the absence of such a comparison it can be argued that the homodyne statistics obtained in some continuous-variable quantum-information experiments are inconclusive [5]. In this paper we make such a direct comparison.

The paper is laid out in the following way. In Sec. II we detail the theoretical relationship between continuous-variable homodyne detection and the direct measurement of average photon flux densities. The experimental approach adopted and the homodyne and single-photon-detector (SPDM) measurement results are described in Sec. III. Finally, a discussion of the significance of the results is given in Sec. IV.

As well as the fundamental interest of our results the demonstrated technique is shown to be easy to add to existing experiments, providing fast measurements over a wide dynamic range. This potentially provides for significant reductions in the time taken to reconstruct the density matricies for qudit systems [6] and other applications in quantum tomography.

II. THEORY

The annihilation and creation operators of an arbitrary field may be expressed in the Heisenberg picture as a sum of the amplitude $\hat{X}_A^+$ and phase $\hat{X}_A^-$ quadrature operators, where the annihilation $\hat{A}$ and creation $\hat{A}^\dagger$ operators are given by [1]

$$\hat{A} = \frac{\hat{X}_A^+ - i\hat{X}_A^-}{2},$$

$$\hat{A}^\dagger = \frac{\hat{X}_A^+ + i\hat{X}_A^-}{2}.$$

The quadrature operators represent continuous-variable observables that are able to be measured via homodyne detection techniques.

If the field operator is expressed as a linear sum of the steady-state coherent amplitude $\bar{A}$ and quantum-mechanical fluctuation terms $\delta\hat{A}(t)$ such that $\hat{A}(t)=\bar{A}+\delta\hat{A}(t)$ and $\hat{A}(t)^\dagger = \bar{A}+\delta\hat{A}(t)^\dagger$, and use is made of the Fourier transform relationship $\delta\hat{A}(t)\rightarrow\delta\tilde{A}(\omega)$ and $\delta\hat{A}(t)^\dagger\rightarrow\delta\tilde{A}(-\omega)^\dagger$, then the power spectrum of the fluctuations of an arbitrary input field can be written [7]

$$V^{\pm}(\omega) = \langle \delta\tilde{A}(\omega)^{\dagger}\delta\tilde{A}(\omega) + \delta\tilde{A}(-\omega)^{\dagger}\delta\tilde{A}(-\omega) \pm \delta\tilde{A}(-\omega)\delta\tilde{A}(\omega) \pm \delta\tilde{A}(-\omega)^{\dagger}\delta\tilde{A}(\omega)^{\dagger}\rangle + 1 \quad (1)$$

where the spectral variance $V^{\pm}(\omega)$ is given by $\langle|\delta X^{\pm}(\omega)|^2\rangle$. The first term of Eq. (1) is the average number of photons $\bar{n}_+$ in the input mode at frequency $+\omega$, the second represents $\bar{n}_-$ at $-\omega$, and the third and fourth represent correlations between the $+\omega$ and $-\omega$ sidebands. The final unit term represents the vacuum fluctuations. In general, this may be expressed as [8]

$$\bar{n}(\omega) = \frac{V^{+}(\omega) + V^{-}(\omega) - 2}{4} \quad (2)$$

where $\bar{n}(\omega)=(\bar{n}_+ + \bar{n}_-)/2$ represents the average number of photons in both the positive and negative sidebands for a continuous variable measurement of the variances at frequency ω. Note that this relationship also remains valid for any pair of orthogonal measurements of the optical phase space, i.e., V^{θ} and $V^{\theta+\pi/2}$. In this case, $V^{\theta}(\omega)=\langle|\delta\tilde{X}^{\theta}(\omega)|^2\rangle$ where $\delta\hat{X}^{\theta}=(\delta\hat{a}e^{i\theta}+\delta\hat{a}^{\dagger}e^{-i\theta})$, representing an arbitrary quadrature operator at angle θ with respect to a specified phase reference.

As a first example consider a coherent state $|\alpha\rangle$. Coherent states can be defined as eigenstates of the annihilation operator, i.e., $\hat{A}|\alpha\rangle=\alpha|\alpha\rangle$. To a good approximation such states can be produced by a well-stabilized laser. We have $V^{+}=4\,\mathrm{Re}(\alpha)^2+1$ and $V^{-}=4\,\mathrm{Im}(\alpha)^2+1$. Using Eq. (2) we find $\bar{n}=\mathrm{Re}(\alpha)^2+\mathrm{Im}(\alpha)^2=|\alpha|^2$ which is as expected.

As another example, consider the homodyne measurement of a squeezed state $|\alpha,r\rangle$. Squeezed states can be defined as eigenstates of the operator $\hat{B}=\sqrt{G}-\sqrt{G-1}$. Such a state possesses the following properties [1]:

$$\Delta X^{+} = e^{-r}, \quad \Delta X^{-} = e^{r},$$

$$\langle N\rangle = |\alpha|^2 + \sinh^2 r,$$

where the squeeze factor $r=-\ln(\sqrt{G}-\sqrt{G-1})$. Assuming a squeezed vacuum state (i.e., $\alpha=0$) with variances V^{+} and V^{-} measured at frequency ω, Eq. (2) yields

$$\bar{n}(\omega) = \frac{|e^{-r}|^2 + |e^{r}|^2 - 2}{4} = \left(\frac{e^{-r} - e^{r}}{2}\right)^2 = |0|^2 + \sinh^2 r,$$

again in agreement with the expected result. The interesting thing in this second example is that the fluctuations in one quadrature can fall below the level associated with no illumination. This example shows that the vacuum noise floor cannot be attributed to technical noise of the detector.

The relationship of Eq. (2) may also be exploited to measure the average photon number in a field of interest using the scheme illustrated in Fig. 1. In order to avoid low-frequency technical noise, an acousto-optic modulator (AOM) [9] introduces a radio-frequency offset ω between the mode of interest and a homodyne detector local oscillator. As shown, the mode of interest is upshifted relative to the local oscillator, and the vacuum mode introduced at frequency $-\omega$ relative to the local oscillator. From Eq. (1), $\langle\delta\tilde{A}(-\omega)^{\dagger}\delta\tilde{A}(-\omega)\rangle=\langle\delta\tilde{A}(-\omega)\delta\tilde{A}(\omega)\rangle=\langle\delta\tilde{A}(-\omega)^{\dagger}\delta\tilde{A}(\omega)^{\dagger}\rangle=0$ and local oscillator phase dependence disappears. Consequently, $V^{+}=V^{-}$ and Eq. (2) yields

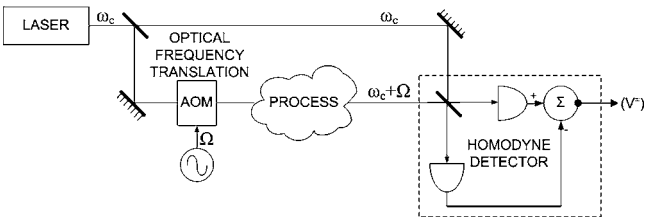

FIG. 1. Generic measurement concept, as applied to determine $\bar{n}$ at the output of an unknown process. The direction of optical frequency translation as performed by the AOM is unimportant, as discussed in the text.

$$\bar{n}_+(\omega) = \langle\delta\tilde{A}(\omega)^{\dagger}\delta\tilde{A}(\omega)\rangle = V(\omega) - 1 \quad (3)$$

where $\bar{n}_+(\omega)$ is the average number of photons in the $+\omega$ sideband. A similar result is obtained if the $+\omega$ and $-\omega$ sidebands are interchanged, i.e., upshifting the local oscillator with respect to the field of interest.

III. EXPERIMENT

To validate the relationship between measurements of the discrete and continuous variable domains indicated by Eq. (3), the experiment of Fig. 2 was constructed. This experiment corresponds to the topology of Fig. 1 where the "process" is that of optical attenuation. The experiment was driven by a Photonetics Tunics-1550 tunable diode laser operated at 1540 nm, the wavelength chosen to permit stable mode-hop-free operation, as well as to take advantage of commercial telecommunications fiber products. The output

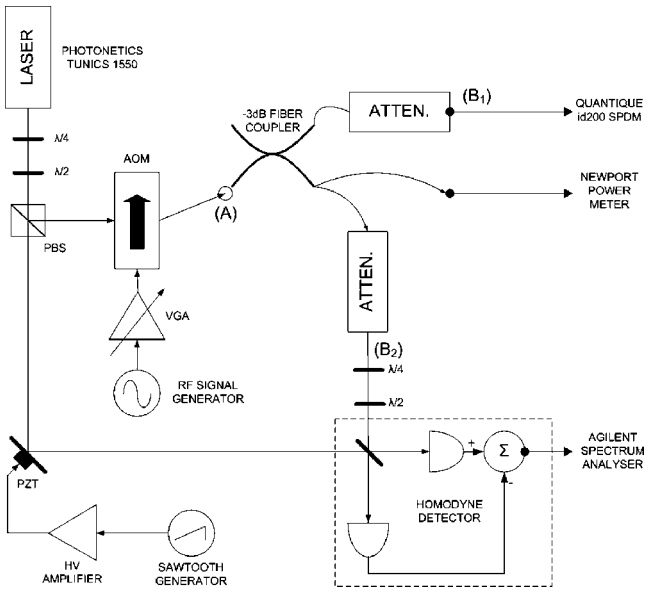

FIG. 2. Schematic representation of the system employed, mode-matching optics omitted for clarity. Points A, B_1, and B_2 represent the states to be measured.

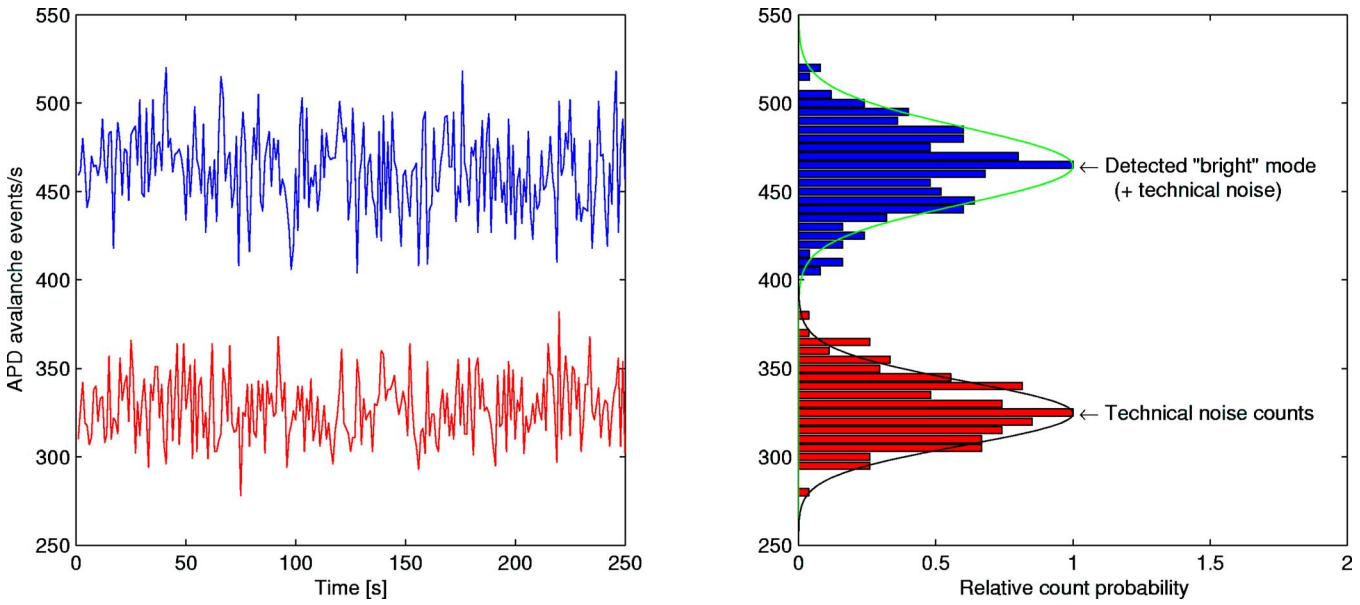

FIG. 3. (Color online) SPDM time series and statistical distributions for $\Phi_A \sim 2 \times 10^7$ photons/s.

beam was divided asymmetrically, the majority of the power used as a coherent local oscillator for the homodyne detector and the remainder upshifted and attenuated to become the field of interest. The field of interest was then measured by three independent detection systems: a homodyne detector, an id-Quantique (id-200) (In,Ga)As/InP SPDM, and a NIST-traceable (Newport 3227) power meter. All interconnections were made with single-mode glass fiber (SMF) in the interests of reproducibility of measurement and for spatial mode filtering.

To permit valid comparisons to be made between the three measurement techniques, all measurements were referred back to point A of Fig. 2, accounting for the losses unique to each optical path in the analysis of results. As physical disturbance of the SMF altered the polarization of the propagating photons via the stress-optic effect [10], a series of data was recorded using a 50-50 fiber coupler to permit simultaneous SPDM and homodyne measurements to be made whereby the signal path wave plates had been previously adjusted for maximum homodyne efficiency. This also made long-time-constant drifts in the laser's output power common to both measurement systems. However, to support the claim that both measurement schemes were truly independent, a small set of results was collected by interchanging the connections of one port of the coupler between the SPDM and the homodyne detector.

Experimentally, measurement of the mean photon number is determined by integrating the mean photon flux Φ over time period τ. The field of interest at point A may be approximated as a weak coherent state $|\alpha\rangle_A$, defined [1] as

$$|\alpha\rangle_A = e^{-|\alpha_A|^2/2} \sum_{n=0}^{\infty} \frac{\alpha_A^n}{\sqrt{n!}} |n\rangle \tag{4}$$

where the mean photon flux is related by $\Phi_A = |\alpha_A|^2 = P_A \lambda / hc$ where P_A is the optical power, λ is the optical wavelength, h is Planck's constant, and c is the speed of light.

$|\alpha\rangle_A$ is further attenuated in a calibrated fashion to yield $|\alpha\rangle_{B_{1,2}}$ with $\alpha_{B_{1,2}}$ varied by adjusting the rf drive power to the AOM to yield values for $\Phi_{B_{1,2}}$ in the range $\sim 10^3 - 10^5$ photons/s. The second-order Bragg-diffracted [11] optical output was used to achieve a greater attenuation than was otherwise possible with the first-order output, and to avoid radiative coupling between the rf signal generator and the homodyne detector. Hence, the AOM was operated at its frequency of peak diffraction efficiency of 80 MHz, and homodyne detection was performed at a center frequency of 160 MHz.

To minimize the statistical uncertainty σ_m associated with N independent experimental measurements as given by $\sigma_m^2 \propto N^{-1}$ [18], N was maximized within practical constraints for both the SPDM and homodyne detection schemes.

After-pulsing probability [12] and long-time-constant laser power drifts imposed a practical maximum value of $\tau = 1$ s (leading to $N = 250$). An APD gating period τ_G of 100 ns was used at 10 μs intervals. The time series for the SPDM shown in Fig. 3 illustrates typical data when the SPDM is illuminated (upper trace) and in the absence of optical input (lower trace). The probability density function of the "bright" data is as described by Eq. (4) and the distribution for the dark counts is also Poissonian in nature [15]. As both distributions are of the same family, the mean of the technical noise may simply be subtracted away [16] to yield the mean number of detection events, provided that the two distributions can be resolved.

The homodyne detector was implemented with matched (In,Ga)As p-i-n photodetectors and an Agilent E4407B spectrum analyzer (SA). Free-space optical components were used to permit independent control of input polarization and relative phase via a piezoelectrical transducer (PZT) mounted mirror. The effective integration time for the homodyne detector is given by $\tau = 1/B$ where B is the resolution

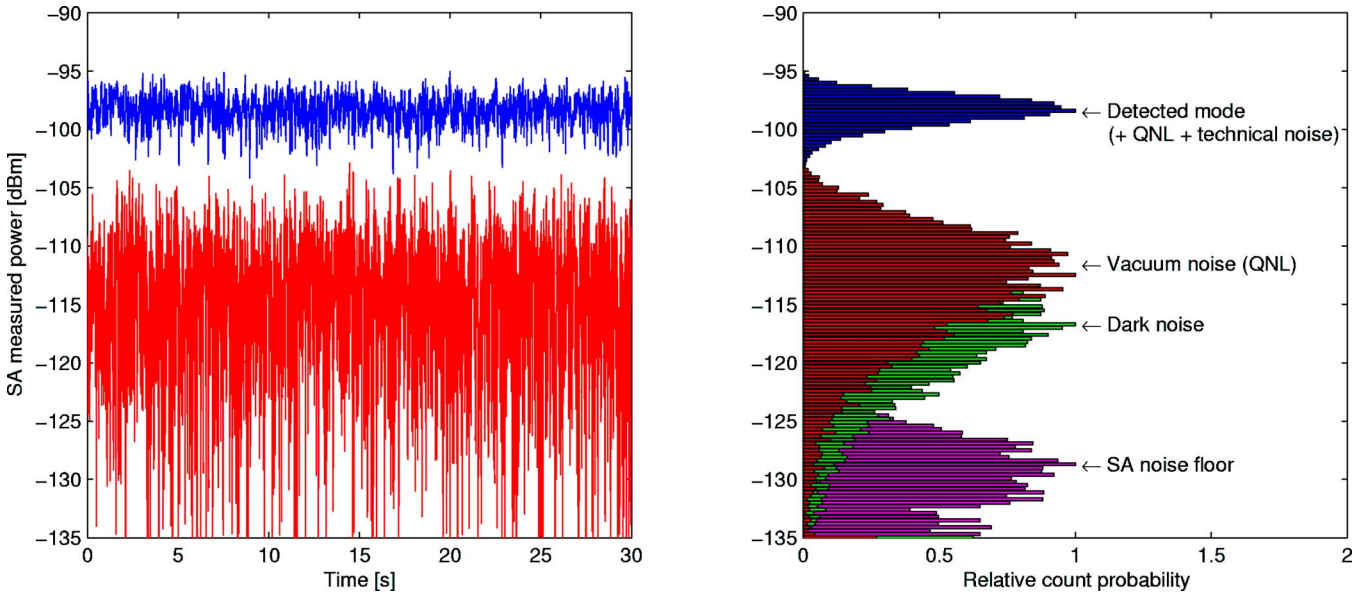

FIG. 4. (Color online) Homodyne detector time series and statistical distributions for $\Phi_A \sim 2\times10^7$ photons/s. For clarity, only the distributions associated with the technical noise sources are illustrated.

bandwidth of the SA. A nominal value of $B=30$ Hz (33.2 Hz measured) was used to yield $\tau=30.1$ ms, with $N=1000$ for a 30 s acquisition period. The overall efficiency of the homodyne detector η is a function of the quantum efficiency η_{det} of the matched *p-i-n* photodetectors and the interferometric fringe visibility $\mathcal{V}$, where $\eta_H=\mathcal{V}^2$ and $\eta=\eta_H\eta_{det}$. Accounting for the transition from fiber to free space, the maximum experimental fringe visibility attained was 93%, giving an overall detection efficiency $\eta=88\%$. Typical time-series data and associated log-Rician [16,17] distributions for the homodyne data are shown in Fig. 4.

Macroscopic power measurements performed by the Newport power meter were used for the purposes of calibrating the incident photon flux into the SPDM and homodyne measurement schemes. Ideally, both schemes would exhibit a linear 1:1 relationship between incident and measured flux over a wide range with a minimum of uncertainty. The extent to which this is achieved is shown in Figs. 5 and 6 where error bars for both axes are placed one standard deviation from the mean, and the solid line represents the ideal 1:1 response. In both plots, data points obtained via the coupler are marked with a point, the circled points (seen at incident fluxes of 1.6×10^5, 8.0×10^6, and 9.8×10^8 photons/s) represent data obtained by interchanging connections as detailed in the preceding section.

Figure 5 illustrates the SPDM inferred mean photon flux, showing a useful linear relationship over approximately three orders of magnitude with the measurement uncertainty increasing rapidly at low light levels. The upper limit is imposed by saturation of the APD gated time bins and the nonlinearity associated with the increasing probability of $\geqslant 2$ photons arriving within each gate window. The lower limit arises as a consequence of the finite dark-count probability and the low observed SPDM quantum efficiency η_S of 11%. Following the correction of dark counts (technical noise) as detailed previously, data points with a negative mean have been deleted and error bars truncated at $\Phi=1$. Note that this process of deletion has also removed one of the circled data values described above.

The homodyne detector results are shown in Fig. 6, the point and circled data values determined via application of Eq. (3) to the measured variances exhibiting a comparatively superior dynamic range in excess of four orders of magnitude. Additionally, close agreement with the ideal 1:1 relationship and the SPDM data trend at all flux levels is observed despite the lack of free experimental parameters. As expected by inspection of Eq. (3), no sensitivity to relative optical phase was observed in the homodyne variance as the

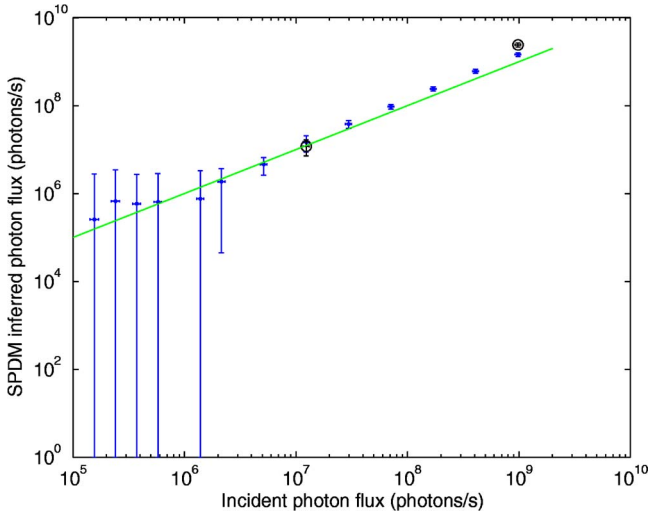

FIG. 5. (Color online) Average photon number at point *A* of Fig. 2, as determined by SPDM measurements. Data values illustrated with a point were obtained using a 50-50 coupler for simultaneous SPDM-homodyne measurements, while circled data points were measured by each scheme separately.

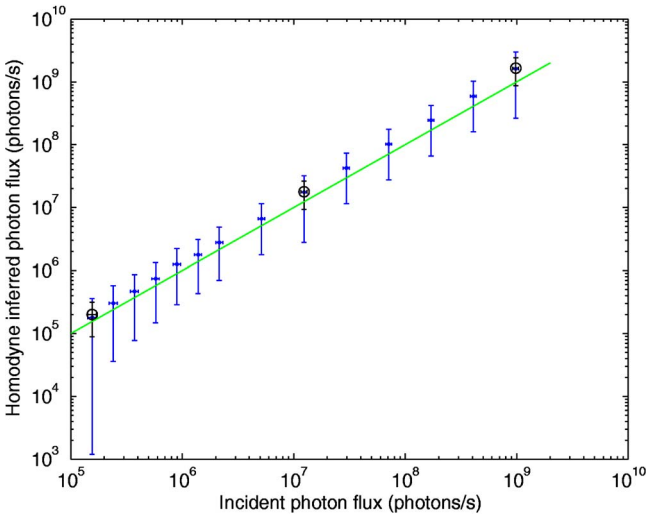

FIG. 6. (Color online) Average photon number at point *A* of Fig. 2, as determined by homodyne detection techniques and quantum mechanics theory. Data values illustrated with a point were obtained using a 50-50 coupler for simultaneous SPDM-homodyne measurements, while circled data points were measured by each scheme separately.

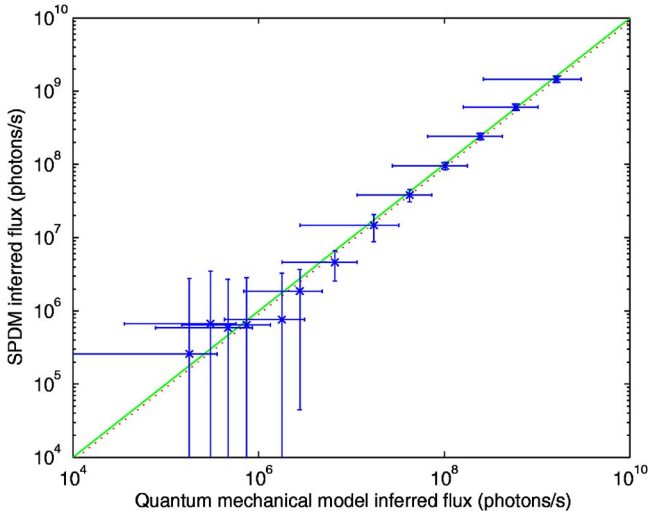

FIG. 7. (Color online) Comparative plot of the SPDM results against the homodyne values determined via quantum mechanics [Eq. (3)]. The solid (green) line indicates the ideal 1:1 relationship, the dotted (red) line indicating the calculated line of best linear fit. Equation for the line of fit is $y=0.9x+0.1$. $\chi^2=0.31$.

PZT illustrated in Fig. 2 was swept over a number of optical wavelengths.

The error bars associated with both the measurement techniques are the result of statistical uncertainties in addition to technical and systematic sources of error. In the SPDM, technical noise manifests itself as undesired count events and missed detection events, these effects becoming dominant at low flux levels.

The SPDM is also insensitive to the input spatial mode and exhibits frequency sensitivity only in response to the bandwidth of the input optics and the spectral responsivity of the semiconductor APD. Experimentally this gave rise to two sources of systematic error: the coupling of ambient room light to fiber cladding modes which could be controlled by shielding the SPDM SMF input, and that due to the AOM isotropically scattering a portion of the (unshifted) input beam and this light being mode matched into the SMF. Reducing the AOM optical input power by changing the preceding beam-splitter ratio reduced the count rates arising from this effect to a level comparable to the APD dark count rate.

Conversely, homodyne detection is inherently sensitive to the spatial mode, polarization, and frequency of the input state to be measured. The resolution bandwith of the SA dictates the frequency selectivity of the technique, with the maximum detection bandwidth determined by the rf components, i.e., the linear photodetectors, subtractor, and SA. As detection is reliant on optical interference at the beam splitter, the spatial and polarization modes of the local oscillator (LO) and signal beams must be identical. This provides a high degree of immunity to the detection of ambient light as such photons are incoherent with either the signal or LO-beam.

Homodyne technical noise is comprised mainly of electronic noise, the primary sources being the SA noise floor and dark noise from the detectors. The subtraction of these noise contributions from the observed variance serves to decrease the precision of the measurement, although this effect may be minimized by increasing the separation between the observed quantum noise limit (QNL) and the technical noise. Assuming fixed amplitude of the electronic noise, the signal to technical noise ratio may be increased by raising the observed power of the QNL. As the detector photocurrent linearly scales with the optical input intensity within limits imposed by saturation [4], this may be readily achieved by raising the local oscillator power.

IV. DISCUSSION

The homodyne detector is a continuous-variable measurement system, and thus is unsuitable for conditioning purposes [13], such as required by nondeterministic qubit operations for the implementation of linear optical quantum computation [14]. Despite this restriction, the results display a useful distinction between the homodyne and SPDM detectors in the photon-counting regime in terms of superior speed, dynamic range, resolution, and input mode sensitivity.

This experiment also permits a comparison to be made between the results of the simultaneous measurement of a given optical field by the two detection techniques. In turn, this allows an examination of two contemporary models of the optical vacuum—quantum mechanics and stochastic electrodynamics. Equation (3) illustrates the relationship between homodyne quadrature variance measurements and photon counting, derived using the principles of quantum mechanics. This relationship is illustrated in Fig. 7, combining the data shown in Figs. 5 and 6. As before, data points with a negative mean have been deleted and error bars have been truncated at $\Phi=1$.

Interestingly, if the subtraction of the vacuum noise contribution is neglected in the derivation of Eq. (3) as required

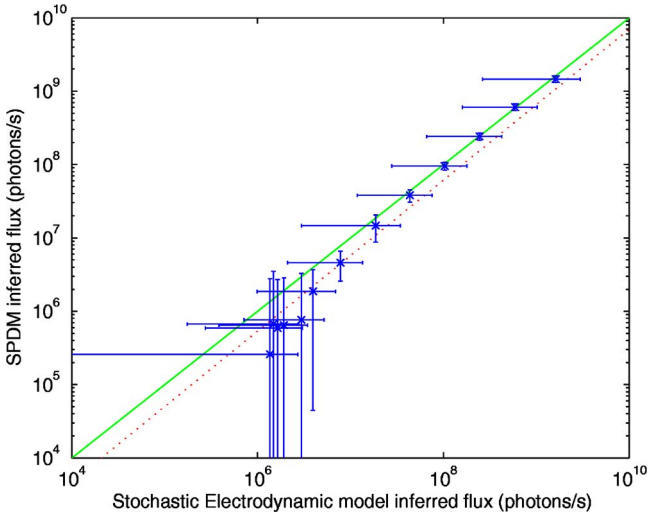

FIG. 8. (Color online) Comparative plot of the SPDM results against the homodyne values determined via stochastic electrodynamics. The solid (green) line indicates the ideal 1:1 relationship, the dotted (red) line indicating the calculated line of best linear fit. Equation for the line of fit is $y=0.7x-28.8$. $\chi^2=1.80$.

by stochastic electrodynamics, then Eq. (3) could be reduced to $\bar{n}(\omega)=V(\omega)$. The values for mean photon number thus derived directly reflect the measured variance, the resulting homodyne data plotted against the SPDM data of Fig. 5 in Fig. 8. It is observed that although the mean magnitudes diverge from the desired 1:1 trajectory at low flux levels, the large experimental uncertainties for the SPDM and homodyne data shown prohibit an unambiguous differentiation between the two models. In order to compare the semiclassical stochastic electrodynamic and quantum-mechanical noise models, the special case of zero-photon input (not shown due to the logarithmic scaling of the plots) must also be considered. Experimentally, this is achieved by blocking the beam to both detectors, the observed homodyne quadrature variance thus declared to be unity and the SPDM only accumulating dark detection events. When the unity variance is scaled by experimental constants the semiclassical model predicts a mean thermal photon flux of 42.6 photons/s, while Eq. (3) returns a value of zero in line with SPDM measurements.

Further quantitative comparison is possible by performing a linear regression analysis of the SPDM and homodyne data for each of the two models. By defining a χ^2 measure of the quality of fit between each data point and the line of fit $y(x)=a+bx$ weighted by the corresponding variances [19] a direct comparison may be made, i.e.,

$$\chi^2(a,b)=\sum_{i=0}^{N-1}\frac{(y_i-a-bx_i)^2}{\sigma_{y_i}^2+b^2\sigma_{x_i}^2}$$

where (x_i,y_i) are the mean data values and $\sigma_{x_i},\sigma_{y_i}$ the associated variances. For the case of zero SPDM flux for the two models, the variances $\sigma_{x_0}=\sigma_{y_0}=1$ were assumed. For the quantum-mechanical case of Fig. 7, the line of fit is given by $y=0.9x+0.1$, $\chi^2=0.31$. For the stochastic electrodynamic model of Fig. 8, the line of fit is given by $y=0.7x-28.8$, $\chi^2=1.80$. Clearly, the quantum-mechanical noise model both permits a superior quality of fit to the observed experimental data and returns an equation for the line of fit closer to the ideal 1:1 relationship.

V. CONCLUSION

We have experimentally verified the proposed homodyne measurement technique and demonstrated a superior sensitivity, dynamic range, and measurement speed than is otherwise possible via linear *p-i-n* photodetectors or APD-based SPDMs. The homodyne detection scheme also offers intrinsic polarization, spatial and frequency selectivity, and in the application presented, does not require elaborate phase locking.

The results of simultaneous quadrature and APD measurements also permit differentiation between semiclassical and fully quantum models of optics. In particular, semiclassical models such as stochastic electrodynamics [20] are unable to account for the observed quadrature variance at the QNL in the absence of photon detection events of the SPDM [8].

ACKNOWLEDGMENTS

J.G.W. gratefully acknowledges the loan of the AOM used within the experiment by Dr. Matt Sellars of the Australian National University and the Tunics laser made available by Dr. David Pulford of the Defence Science and Technology Organisation. This work was supported by the Australian Research Council.

[1] D. F. Walls and G. J. Milburn, *Quantum Optics* (Springer-Verlag, Berlin, 1995).
[2] G. Zambra, A. Andreoni, M. Bondani, M. Gramegna, M. Genovese, G. Brida, A. Rossi, and M. G. A. Paris, Phys. Rev. Lett. **95**, 063602 (2005).
[3] D. M. Pozar, *Microwave Engineering*, 2nd ed. (John Wiley & Sons, Toronto, 1998).
[4] H-A. Bachor and T. C. Ralph, *A Guide to Experiments in Quantum Optics*, 2nd ed. (Wiley-VCH, Weinheim, 2004).
[5] C. M. Caves and K. Wodkiewicz, Phys. Rev. Lett. **93**, 040506 (2004).
[6] R. T. Thew, K. Nemoto, A. G. White, and W. J. Munro, Phys. Rev. A **66**, 012303 (2002).
[7] E. H. Huntington, G. N. Milford, C. Robilliard, T. C. Ralph, O. Glöckl, U. L. Andersen, S. Lorenz, and G. Leuchs, Phys. Rev. A **71**, 041802(R) (2005).
[8] T. C. Ralph, W. J. Munro, and R. E. S. Polkinghorne, Phys. Rev. Lett. **85**, 2035 (2000).
[9] A. Korpel, Proc. IEEE **69**, 48 (1981).
[10] B. A. E. Saleh and M. C. Teich, *Fundamentals of Photonics* (Wiley, New York, 1991).
[11] E. H. Young and S-K. Yao, Proc. IEEE **69**, 54 (1981).

[12] D. Stucki, G. Ribordy, A. Stefanov, H. Zbinden, J. G. Rarity, and T. Wall, J. Mod. Opt. **48**, 1967 (2001).
[13] K. Nemoto and S. L. Braunstein, Phys. Rev. A **66**, 032306 (2002).
[14] E. Knill, L. Laflamme, and G. J. Milburn, Nature (London) **409**, 46 (2001).
[15] X. Sun and F. M. Davidson, J. Lightwave Technol. **10**, 1023 (1992).
[16] Agilent Technologies, Technical Report No. 5966-4008E, 2003 (unpublished).
[17] D. A. Hill and D. P. Haworth, IEEE Trans. Instrum. Meas. **39**, 432 (1990).
[18] P. R. Bevington and D. K. Robinson, *Data Reduction and Error Analysis for the Physical Sciences*, 2nd ed. (WCB/McGraw Hill, New York, 1992).
[19] W. H. Press *et al.*, *Numerical Recipes in C: The Art of Scientific Computing*, 2nd ed. (Cambridge University Press, Cambridge, England, 1992).
[20] T. W. Marshall and E. Santos, Phys. Rev. A **41**, 1582 (1990).